batteries

MDPI

Article

Modelling of Battery Energy Storage Systems Under Real-World Applications and Conditions

Achim Kampker [1], Benedikt Späth [1,*], Xiaoxuan Song [1,2,*] and Datao Wang [2]

[1] Chair of Production Engineering of E-Mobility Components (PEM), RWTH Aachen University, 52072 Aachen, Germany
[2] Huawei Technologies Duesseldorf GmbH, 40549 Düsseldorf, Germany
* Correspondence: b.spaeth@pem.rwth-aachen.de (B.S.); xiaoxuan.song@rwth-aachen.de (X.S.)

Abstract

Understanding the degradation behavior of lithium-ion batteries under realistic application conditions is critical for the design and operation of Battery Energy Storage Systems (BESS). This research presents a modular, cell-level simulation framework that integrates electrical, thermal, and aging models to evaluate system performance in representative utility and residential scenarios. The framework is implemented using Python and allows time-series simulations to be performed under different state of charge (SOC), depth of discharge (DOD), C-rate, and ambient temperature conditions. Simulation results reveal that high-SOC windows, deep cycling, and elevated temperatures significantly accelerate capacity fade, with distinct aging behavior observed between residential and utility profiles. In particular, frequency modulation and deep-cycle self-consumption use cases impose more severe aging stress compared to microgrid or medium-cycle conditions. The study provides interpretable degradation metrics and visualizations, enabling targeted aging analysis under different load conditions. The results highlight the importance of thermal effects and cell-level stress variability, offering insights for lifetime-aware BESS control strategies. This framework serves as a practical tool to support the aging-resilient design and operation of grid-connected storage systems.

Keywords: BESS; lithium-ion battery modeling; thermal–aging coupling

Academic Editors: Muhammed Cavus, Margaret Carol Bell and Pascal Venet

Received: 1 September 2025
Revised: 20 October 2025
Accepted: 21 October 2025
Published: 24 October 2025

Citation: Kampker, A.; Späth, B.; Song, X.; Wang, D. Modelling of Battery Energy Storage Systems Under Real-World Applications and Conditions. *Batteries* **2025**, *11*, 392. https://doi.org/10.3390/batteries11110392

1. Introduction

Stationary lithium-ion batteries have an enabling function for integrating intermittent renewables and providing grid services [1]. The stationary BESS market has grown strongly, with applications ranging from grid-assisted services like frequency modulation to customer-level solar self-consumption [2]. This wide range of applications—from peak shaving and price arbitrage to residential solar offset—makes direct comparisons and standard evaluation difficult [3]. Compared with the automotive industry (which uses standard drive cycles), stationary storage lacks a standard use case [4] and, therefore, requires realistic simulation under representative load profiles to assess technical and economic performance.

Battery degradation strongly depends on operating conditions: high currents (C-rate), deep cycling, high SOC, and high temperature all accelerate aging [5,6]. Therefore, accurate lifetime estimation requires simulating the way that a given load profile drives cell stress over multiple cycles. Simplified assumptions (e.g., constant cycling) can underestimate or miss important effects. For example, Leng et al. (2015) demonstrated that elevated

temperatures (25–55 °C) increase the rate of capacity fade in Li-ion batteries, largely owing to electrode film growth and impedance rise, particularly under high current cycling [7]. Recent works build on this: a multi-stage aging dataset by Stroebl et al. (2024) show that both cycle count and calendar time contribute measurably to capacity loss even under moderate SOC swings, temperature, and C-rates [8]. Similarly, Roy et al. (2024) provide evidence that increasing discharge rates from 0.5C to 0.8C at 25 °C reduce cycle life by over 50%, highlighting non-linear effects of C-rate on aging [9]. In addition, a review by Madani et al. (2025) quantified the combined influence of temperature, DOD, and C-rate in empirical cycles across many commercial lithium iron phosphate (LFP)/graphite cells, finding that high DOD and high–average SOC drive disproportionately faster degradation [10].

To address these challenges, holistic simulation platforms have been developed. SimSES (v15.09.2024) is an open-source Python (v3.13) framework designed for time-series techno-economic analysis of BESS. SimSES is founded upon an extensible, modular architecture that enables extensive topology and component options along with detailed techno-analysis and -economics [11]. The current approach extends SimSES and develops a detailed multi-physics BESS simulation that connects electrical equivalent circuit models with thermal networks and aging algorithms. This paper describes an extensible Python-based framework and its application using realistic load profiles, demonstrating its ability to reproduce known degradation modes under different stress conditions. While SimSES provides a robust techno-economic framework with integrated cell models and empirical aging functions, its main focus lies on system-level analysis. In contrast, the present work develops a Python-based framework that emphasizes cell-level detail: (i) a semi-empirical aging model parameterized for LFP cells, (ii) an RC-based electrical sub-model that captures dynamic voltage response, and (iii) a modular integration of electrical, thermal, and aging processes. This design enables transparent parameterization and direct experimental validation, offering more interpretability than existing black-box approaches. Validation against constant–current cycling confirms good agreement in both voltage (<15 mV RMSE) and temperature (<1 °C RMSE). The framework thus provides a flexible basis for aging-aware BESS evaluation under realistic operating scenarios.

2. Methods

In order to achieve the main goal of this research—to develop a robust framework for simulating the performance of BESS under real conditions—a comprehensive methodology was adopted. The methodology integrates empirical modeling, data-driven simulation, and advanced data analysis techniques. From Figure 1, these methods were structured to address each specific research objective as follows:

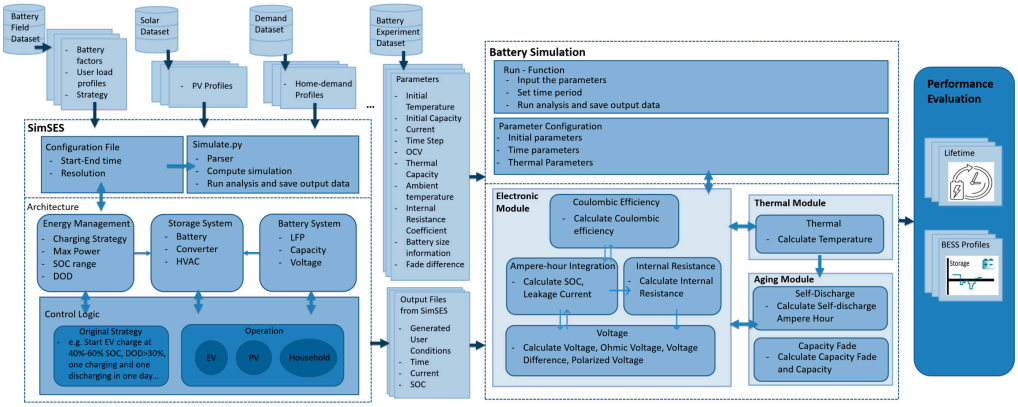

Figure 1. Methodology process diagram.

2.1. Generation of Real-World Load Profiles

To generate representative load profiles for BESS applications from stress factor distributions and features observed under real-world work conditions, data-driven and empirical energy system modeling was employed. These approaches include the use of look-up tables and empirical models derived from the open-source simulation framework SimSES to simulate real-world load profiles. All relevant components of an energy system are considered, such as photovoltaic, households, power converters, grid, etc. These models will be extended in the research by injecting different operating condition features to accurately simulate load dynamics under various usage scenarios. There are two representative scenarios: residential PV-coupled home energy systems and utility-scale applications. The residential profile is derived from anonymized household consumption data with added PV production (midday generation and evening discharge). The utility profile simulates a commercial load with different peaks (e.g., peak shaving, microgrid, and frequency modulation). These curves are generated over time and ensure realistic features such as daily peaks, weekday/weekend variations, and seasonal trends.

2.2. The Lithium-Ion Battery Simulation Model

A modular, Python-based battery simulation framework that integrates electrical, thermal, and aging sub-models was developed. The electrical model is based on an equivalent circuit approach, incorporating open-circuit voltage (OCV) characteristics, ohmic resistance. The thermal model considers reversible (entropy), irreversible (resistance) thermal effects, and dissipation through thermal resistance and capacitance.

A semi-empirical aging model controls capacity fade and internal resistance growth. Cycling degradation is modeled as a function of charge throughput and ΔSOC, while calendar aging follows the temperature-dependent Arrhenius law. All sub-models interact bidirectionally, e.g., temperature feeds back into degradation rates. This integrated approach ensures that stress factors such as SOC, C-rate, temperature, and DOD jointly influence aging outcomes, reflecting the cell-to-cell variations, thus enabling a realistic simulation of the degradation dynamics of the battery system.

2.3. Scenario-Based Simulation and Validation

The overall simulation is structured around timestep integration. At each time step, the target power is applied from the synthesized profile, and battery voltage, temperature, and degradation state are updated in sequence. The simulation tracks both cell-level and pack-level outputs like energy throughput, efficiency, and capacity metrics.

In performance and trend analysis for battery aging, statistical technologies such as time-series analysis and data visualization (e.g., violin plots, heatmaps) were utilized. Simulation results were also compared with experimental datasets to evaluate the precision, especially in voltage and thermal dynamics for various SOC and C-rate conditions.

3. Modeling Framework

To analyze the long-term degradation behavior of lithium-ion BESS under realistic conditions, a modular simulation framework was developed. The framework combines a physics-informed battery model with empirical aging mechanisms and enables the simulation of different application scenarios using real-world load profiles. Implemented in Python, the framework supports rapid scenario generation, component customization, and parameter variability analysis.

3.1. Overall Simulation Architecture

To capture the lifetime behavior of BESS under real-world operational conditions, a hierarchical and modular Python-based simulation framework was developed. This framework expands upon a validated LFP battery model to simulate full BESS operation, integrating system-level scheduling, cell-level physical behavior, and realistic variability.

As illustrated in Figure 2, the simulation is composed of two main layers: the system layer (BESS simulation manager) and the battery layer (pack/cell sub-models). At the top level, a control module named "structure_combine" coordinates the entire BESS simulation. It acts as the scheduler, linking scenario-level input data, such as load profiles, ambient conditions, and duration, with the battery sub-models. This control layer also handles cell parameter initialization and assigns variability among individual cells using a dedicated "Initdata" class.

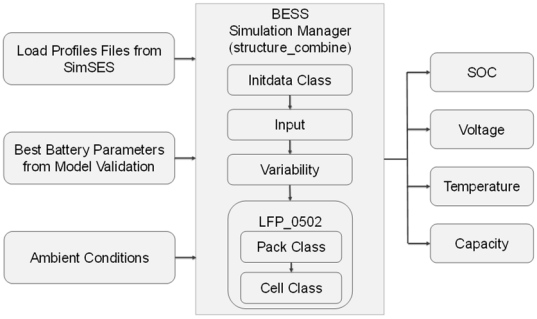

Figure 2. BESS simulation framework schematic.

3.1.1. BESS Input Configuration

Each simulation scenario is defined by a set of realistic load conditions derived from open-source grid-scale models SimSES. These include:

- Current vs. Time Profiles: Time-resolved charge/discharge patterns at the system level.
- Ambient Conditions: Temperature and cooling assumptions.
- Initial Settings: SOC, capacity, resistance, and temperature, with user-defined spread.
- Simulation Parameters: Time step, run duration, save intervals.

To reflect cell-to-cell variability, the "Initdata" class samples slightly different initial parameters per cell, including SOC, capacity, resistance, and initial temperature. These distributions are calibrated based on field data provided by industry partners, ensuring a non-homogeneous pack representation.

3.1.2. Simulation Execution Flow

Once initialized, the "structure_combine" module dispatches simulation tasks across the pack. Each virtual cell is independently simulated by invoking the Pack and Cell classes, which comprise the core electro-thermal–aging models. These models operate on 10s resolution and track each cell's SOC, terminal voltage, cell temperature, and capacity.

This cell-level data is collected, stored, and exported for each simulation case, enabling scenario-level statistical analysis of degradation, energy throughput, thermal behavior, and cell divergence.

3.1.3. Modularity and Scalability

Each cell object comprises three key submodules:

- Electrical module: OCV-R-based voltage model with rate-sensitive surface SOC correction.
- Thermal module: Collective parameter model capturing heat generation and dissipation.
- Aging module: Semi-empirical degradation sub-models based on cycling and calendar effects.

- Variability injection: Parameter distributions handled externally for statistical batch simulation.

The framework also supports extension of other BESS-level elements (e.g., inverter efficiency models, HVAC modules, control algorithms), making it suitable for broader techno-economic or multi-domain simulation studies.

3.2. Electrical Module

The cell-level electrical behavior is represented using an equivalent circuit model (ECM) composed of an ohmic resistance R0 model, a parallel RC branch (R1, C1), and the OCV curve as a function of SOC. The OCV-R0 model captures the static voltage response, while the RC branch accounts for short-term polarization and surface SOC dynamics under transient current conditions. This design ensures that dynamic overpotentials and Joule heating are realistically represented, which are important drivers of thermal rise and subsequent degradation, even though the RC dynamics are not directly linked to long-term aging. SOC integration is computed using Coulomb counting with Coulombic efficiency factors for charging/discharging.

Parameterization of R0, R1, C1 and the OCV curve was performed using laboratory galvanostatic pulse-relaxation tests on an LFP/graphite cell. Current pulses were applied at different SOC levels and the relaxation phases were used to resolve polarization and resistance components. Curve fitting was conducted using Python SciPy non-linear least squares algorithms, ensuring consistency with electrochemical response.

An additional simplified equivalent element capacitor model (EECM) was integrated in series with the RC block to reproduce short-term diffusion lag at high current transients. This element is not a physical capacitor but a phenomenological representation to improve fidelity under dynamic load profiles.

3.3. Thermal Module

Thermal dynamics are captured using a lumped-parameter model, accounting for reversible and irreversible heat generation and limited cooling via convection [12]:

$$Qirrev(t) = I(t) \cdot \Delta U \tag{1}$$

$$Qrev(t) = I(t) \cdot T \cdot \delta(SOC) \tag{2}$$

$$Qloss = h \cdot A \cdot (T - T_{amb}) \tag{3}$$

$$T(t + \Delta t) = T(t) + \frac{Qirrev + Qrev - Qloss}{mc_p} \tag{4}$$

where Qloss describes heat dissipation through simplified convective cooling. The model tracks internal cell temperature evolution and feeds it back into both the electrical and aging modules, enabling temperature-dependent behavior.

Temperature is updated for each cell at every timestep, with heat capacity c_p, mass m, surface area A, and heat transfer coefficient h defined as cell-specific constants. This module enables a realistic prediction of thermal rise during high C-rate discharges or poor cooling conditions.

3.4. Aging Module

Long-term degradation is modeled using a semi-empirical approach adapted from Wang et al. [13]. Although more recent empirical functions are integrated within SimSES, this formulation was deliberately chosen for two reasons. First, it enables consistent parameterization with the experimental dataset available for the selected LFP cells, thereby ensuring a coherent validation procedure across electrical, thermal, and aging modules.

Second, the model structure, explicitly linking temperature, C-rate, and DOD, facilitates its adaptation to time-varying profiles through numerical integration, which is less transparent in black-box empirical fits. This model considers both calendar aging and cycling aging, with sensitivities to key factors such as temperature, C-rate, range of SOC fluctuation, and DOD. Although the original work is based on constant current and temperature conditions, it is adapted here for time-varying simulation using trapezoidal integration. The rate of capacity degradation dQloss/dt is expressed as

$$\frac{dQ_{loss}}{dt} = \left(\frac{15}{C_{rate}}\right)^{\frac{1}{3}} \cdot 10000 \cdot e^{(-31700 + 370.3 \cdot C_{rate})/R \cdot T} \cdot 0.55 \cdot Ah^{-0.45} \cdot C_{rate}{}^{\frac{2}{3}} \quad (5)$$

Cycling degradation is expressed as a function of cumulative charge throughput (Ah) and SOC range. Although ΔSOC does not appear explicitly in the simplified form of Equation (5), its effect is embedded in the charge throughput and cycling amplitude terms. Here, Ah denotes the integrated current over time, normalized to ampere-hours.

Calendar degradation follows a temperature-dependent Arrhenius relationship, with activation energy calibrated for LFP systems. The reversible (entropic) and irreversible (ohmic) contributions to heat generation are considered, with the entropic coefficient δ(SOC) approximated from literature data [13] and included to account for reversible heat effects.

Resistance growth due to aging is applied to the ohmic resistance R0, representing electronic and ionic transport losses, while R1 in the RC branch is kept constant since it primarily serves to capture short-term polarization rather than aging effects. This approach allows a realistic link between accumulated stress factors and their manifestation in increased ohmic loss and reduced available capacity.

3.5. Model Validation

The developed ECM–thermal–aging framework was validated against laboratory cycling data obtained from commercial LFP cells (nominal capacity 280 Ah). Tests included constant current charge/discharge at C-rates from 0.1C to 1C under controlled ambient temperature (25 °C). The simulation was configured with fixed initial parameters (capacity, resistance, thermal constants), and only the initial SOC was varied across test segments.

- Electrical validation:
  The ECM parameters (R0, R1, C1) were fitted using current pulse and CC cycling data. Voltage prediction was benchmarked against experimental results, yielding RMSE below 15 mV over the full SOC range, with increased error (~37 mV) only near 95–98% SOC, where OCV slope is steep.
- Thermal validation:
  Thermal parameters (mass, heat capacity, surface area, heat transfer coefficient) were obtained from manufacturer data and calibration tests. Simulated temperature rise closely followed experimental trends, with RMSE < 1.0 °C across all C-rates.
- Integration check:
  The validated ECM and thermal modules were then coupled with the aging module to ensure consistent feedback of temperature- and SOC-dependent behavior.

This validation confirms that the model reliably reproduces both steady-state and transient cell responses, forming a robust basis for long-term BESS degradation simulations.

Figures 3 and 4 illustrate representative comparisons of voltage and temperature profiles under different C-rates for both charging and discharging. The simulation captures key dynamic behaviors, such as voltage plateaus and thermal rise, with strong consistency across SOC levels and current conditions.

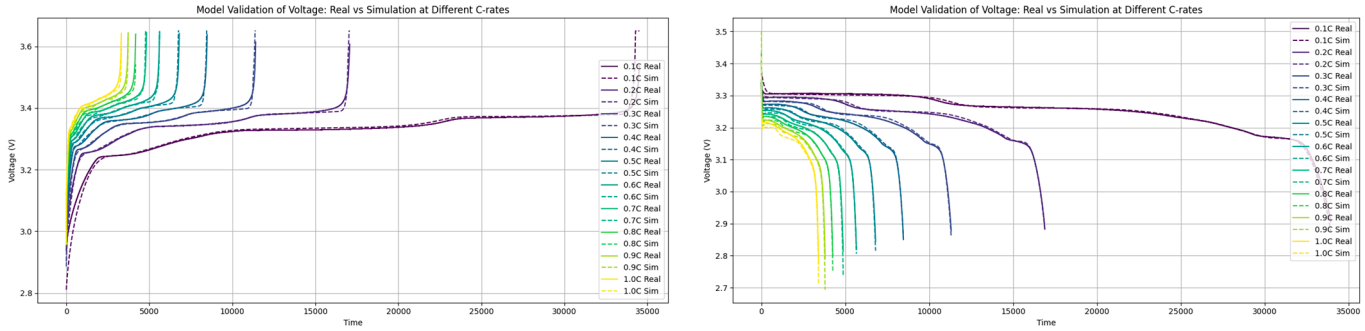

(**a**) (**b**)

Figure 3. Voltage comparison. Real vs. simulation at different C-rates: (**a**) voltage comparison at charging segments; (**b**) voltage comparison at discharging segments.

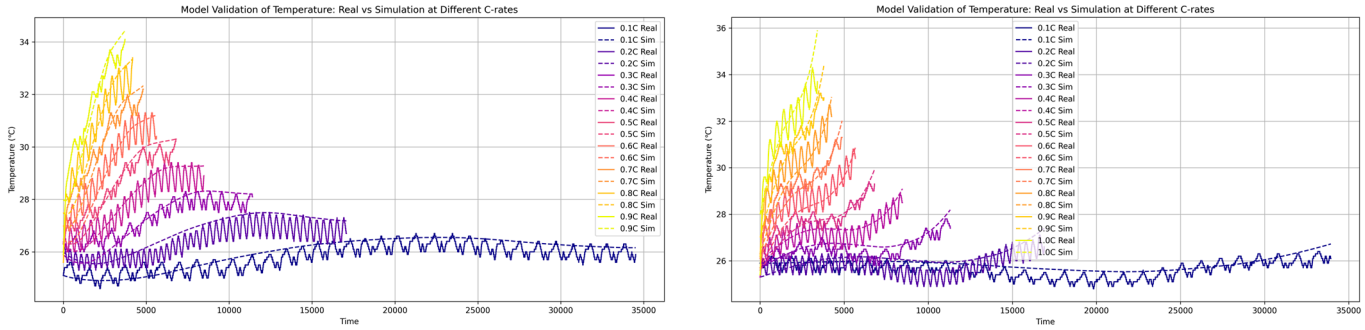

(**a**) (**b**)

Figure 4. Temperature comparison. Real vs. simulation at different C-rates: (**a**) temperature comparison at charging segments; (**b**) temperature comparison at discharging segments.

Quantitatively, RMSE was calculated across four SOC intervals:

Voltage prediction: RMSE remained less than 15 mV over the full 0–100% SOC range, with most intervals (10–35% and 35–95%) achieving sub-10 mV accuracy. Notably, a slight error increase (up to ~37 mV) was observed near the 95–98% SOC range at high C-rates, due to steeper OCV slopes and increased resistance effects.

Temperature prediction: Across all C-rates, the thermal model achieved RMSE < 1.0 °C, with best accuracy (RMSE < 0.5 °C) in the 35–95% SOC range. Slightly higher errors occurred during initial charging stages (10–35% SOC) due to rapid Joule heating and transient thermal lag.

These results demonstrate the model's reliability in reproducing both electrical and thermal responses across a wide operating envelope, validating its use in long-term, real-world scenario simulations.

4. Results

To evaluate the impact of real-world load profiles on battery degradation, the proposed BESS model was simulated under multiple utility-scale and residential-scale operating scenarios. For each condition, simulations were performed using a simplified pack of two series-connected cells with parameter-level variability introduced to reflect experimental inconsistency. Twenty samples per condition were generated to capture statistical variation. Each scenario was simulated at four ambient temperatures (10 °C, 25 °C, 45 °C, and 60 °C), and capacity retention was assessed over a 30-day or 90-day operation period, depending on use case characteristics.

Tables 1 and 2 summarize the key simulation outcomes, including charge/discharge rates, DOD ranges, SOC bands, voltage behavior, and resulting capacity retention at differ-

ent temperatures. These results reflect the cumulative aging effect induced by both cycling and temperature stress, while time-domain behavior- and sample-specific trajectories are omitted here for brevity.

Table 1. Summary of utility conditions: mean range of voltage, current, SOC, DOD, and average capacity retention.

Conditions	Charge C-Rate	Discharge C-Rate	DOD Range	Main SOC Range	Voltage Distribution	Duration	Retention at 10 °C	Retention at 25 °C	Retention at 45 °C	Retention at 60 °C
Peak Shaving	~0.5C	~0.2C–0.5C	90–100%	0–100%	~2.6 V–3.6 V	30 Days	98.8%	97.9%	96.3%	95.4%
Microgrid with high DOD	~0.1C	~0.01C	75–95%	0–100%	~2.95 V–3.5 V	30 Days	98.9%	97.8%	95.5%	93.0%
Microgrid with low DOD	~0.1C	~0.1C	45–65%	~40–70%	~3.24 V–3.38 V	30 Days	99.2%	98.4%	96.7%	94.6%
Frequency modulation with high DOD	~0.5C	~0.001C	55–80%	~40–100%	~3.25 V–3.5 V	30 Days	99.2%	98.6%	97.4%	96.0%
Frequency modulation with low DOD	~0.3C	~0.001C	25–30%	~80–100%	~3.2 V–3.45 V	30 Days	99.4%	98.9%	97.9%	96.7%

Table 2. Summary of residential conditions: mean range of voltage, current, SOC, DOD, and average capacity retention.

Conditions	Charge C-Rate	Discharge C-Rate	DOD Range	Main SOC Range	Voltage Distribution	Duration	Retention at 10 °C	Retention at 25 °C	Retention at 45 °C	Retention at 60 °C
Deep charge and discharge	~0.2C	~0.1C	85–100%	0–100%	~2.8 V–3.65 V	30 Days	98.0%	96.1%	91.2%	85.0%
						90 Days	96.3%	92.8%	84.0%	72.5%
Semi-deep charge and discharge	~0.15C	~0.04C	~80%	~15–100%	~3.15 V–3.38 V	30 Days	98.0%	96.1%	91.3%	85.0%
High-SOC cycle	~0.035C	~0.01C	25–30%	~70–100%	~3.28 V~3.65 V	30 Days	98.6%	97.2%	93.7%	89.2%
						90 Days	97.3%	94.8%	88.4%	80.0%
Medium–high-SOC cycle	~0.15C	~0.02C	55–60%	~40–100%	~3.24 V~3.6 V	30 Days	98.2%	96.4%	92.0%	86.3%
						90 Days	96.6%	93.4%	85.3%	74.7%
Medium- and low-SOC cycle	~0.09C	~0.02C	45–55%	~10–70%	~3.18 V–3.37 V	30 Days	98.2%	96.5%	92.2%	86.7%
Low-SOC cycle	~0.08C	~0.015C	20–30%	~15–40%	~3.16 V–3.325 V	30 Days	98.6%	97.2%	93.7%	89.2%
						90 Days	97.3%	94.8%	88.3%	80.0%

4.1. Utility-Scale Scenarios

Five utility-relevant load cases were simulated to emulate grid-oriented BESS applications such as peak shaving, microgrid support, and frequency modulation. As shown in Table 1, capacity retention after 30 days of simulated operation ranged from 99.4% (low-DOD frequency modulation) to 93.0% (high-DOD microgrid), with aging trends strongly influenced by discharge depth and cell voltage range.

4.2. Residential-Scale Scenarios

Six residential use cases were evaluated to represent various solar self-consumption and home backup behaviors, characterized by different SOC bands and cycling depths.

Table 2 presents the aging results over both 30-day and 90-day durations. Deep and semi-deep cycling at high DOD and wide SOC range caused the most severe capacity fade, up to 15% over 90 days at 60 °C. In contrast, low-DOD, high-SOC cycles showed reduced degradation under the same thermal stress.

5. Discussion

The simulation results presented in Section 3 reveal distinct degradation trends under different real-world BESS use cases. This section discusses the key influencing factors, comparative analysis between utility and residential scenarios, and implications for model application and system design.

5.1. Impact of Depth of Discharge and Temperature

Across both utility and residential scenarios, DOD emerged as a dominant factor in capacity fade. Use cases involving high DOD, such as deep charge/discharge in residential settings and microgrid support with high DOD in utility scenarios, exhibited accelerated degradation. For instance, in the residential deep cycling case, capacity retention dropped to 72.5% after 90 days at 60 °C, indicating a compounding effect of thermal stress and deep cycling.

Conversely, low-DOD cycles, especially under high-SOC bands (e.g., frequency modulation and high-SOC residential cycling), resulted in relatively minor capacity fade (<5% at 60 °C in 30 days). These results align with experimental findings in the literature, reinforcing the validity of the implemented semi-empirical aging model.

In all cases, temperature played a critical role, amplifying both calendar- and cycle-induced degradation. While 10 °C and 25 °C yielded minimal fade (<3%), high-temperature cases (45–60 °C) showed significant retention loss, especially in scenarios with high voltage exposure and long dwell times at full charge. These results highlight the importance of thermal management, particularly in warmer climates or poorly ventilated installations.

5.2. Operational Profile Characteristics and Aging Behavior

The SOC operating window also influenced aging. Cycles confined to the mid-to-high-SOC range tended to cause greater resistance growth and fade than mid-range operations with limited voltage stress. This behavior can be attributed to electrochemical stress mechanisms at high SOC. Operating close to the upper voltage limit increases electrode potential, which promotes electrolyte oxidation and transition-metal dissolution, thereby accelerating SEI growth and impedance rise. Recent experimental work in LFP cells confirms that voltage cutoff (i.e., maximum SOC/voltage limit) is among the top aging factors, nearly as important as temperature under many cycling protocols [14]. Large SOC swing combined with high average SOC increases capacity fade even under moderate C-rate and temperature conditions [15]. Moreover, the recent review by Wang et al. (2025) synthesized evidence that elevated SOC windows (especially above ~80–90%) lead to non-linear increases in parasitic side reactions and loss of lithium inventory [16]. Consequently, the high-SOC cycle in residential applications showed greater degradation than the medium–low-SOC cycle, despite involving a smaller DOD. Charge/discharge rate asymmetry was another subtle yet impactful factor. Cases with slow discharge and moderate charging (e.g., frequency modulation and home backup) exhibited better retention than profiles involving sustained or rapid discharges, even at similar DOD. This supports the observation that current-induced overpotentials and heating during discharge play a role in accelerating degradation mechanisms such as lithium plating or SEI growth.

5.3. Utility vs. Residential Scenario Comparison

Overall, residential scenarios exhibited more severe aging compared to utility use cases. This is primarily due to higher average DOD, especially in self-consumption and daily deep cycling, more time spent at high SOC or voltage, and longer durations and higher operating temperatures in some configurations.

For example, while frequency modulation in the utility case involved shallow cycles, its total energy throughput and temperature exposure were modest, resulting in <4% capacity loss even at 60 °C. In contrast, deep residential cycles resulted in >15% capacity loss at the same temperature over longer durations.

These findings suggest that residential BESS deployments are more susceptible to rapid degradation, especially when operated without thermal or usage optimization. This underscores the importance of adaptive control strategies and potentially revised warranty models in behind-the-meter applications.

5.4. Model Utility and Limitations

The simulation framework successfully captured the interplay between electrical load dynamics, thermal conditions, and aging responses. Its modular structure allows for flexibility in scenario configuration and facilitates use in early-stage design assessment or operational planning. However, limitations exist. The current aging model does not capture:

- Gas evolution or swelling effects.
- Electrolyte decomposition.
- Effects of BMS balancing or thermal runaway risk in abnormal events.

Additionally, the simplified pack configuration (two-cell model) may not fully reflect large-scale pack-level heterogeneity or thermal gradients. Future work may extend the framework to integrate multi-cell thermal coupling, real-world temperature sensors, and state estimation algorithms.

6. Conclusions

This paper presents a modular, physics-informed simulation framework for analyzing lithium-ion battery degradation in BESS under realistic residential and utility operating conditions. Through the incorporation of the electrical, thermal, and aging sub-models into a Python-cell-level simulation framework, the architecture provides for high-resolution monitoring of the voltage, SOC, temperature, and capacity fade under dynamic load profiles.

Simulation results verify that degradation is strongly affected by key operational parameters such as SOC window, DOD, C-rate, and temperature. In utility-scale scenarios, aggressive cycling, such as high-DOD frequency modulation, induces faster aging compared to microgrid or low-DOD conditions. Similarly, residential use cases with deep or semi-deep cycle operating conditions at the high-SOC ranges exhibit rapid capacity fade, especially at high temperatures. Multi-case study analysis also demonstrates the role played by inconsistency on the cell level and thermal stress in increasing aging, emphasizing the importance of managing both electrical and thermal operating conditions.

The proposed framework not only enables scenario-driven aging analysis but also provides interpretable outputs through time-series visualization, capacity retention heatmaps, and summary metrics. These features support actionable insights into aging-aware operation and design of BESS. Future work will extend the framework to include system-level controls, larger-scale pack simulation, and long-term degradation forecasting for techno-economic analysis.

Author Contributions: Conceptualization, B.S. and X.S.; methodology, B.S. and X.S.; investigation, B.S. and X.S.; writing—original draft, B.S. and X.S.; writing—review and editing, A.K. and D.W.; supervision, A.K. All authors have read and agreed to the published version of the manuscript.

Funding: This research received no external funding.

Data Availability Statement: The data presented in this study are available on request from the corresponding authors.

Conflicts of Interest: Authors Xiaoxuan Song and Datao Wang were employed by the company Huawei Technologies Duesseldorf GmbH. The remaining authors declare that the research was conducted in the absence of any commercial or financial relationships that could be construed as a potential conflict of interest.

Abbreviations

The following abbreviations are used in this manuscript:

BESS	Battery Energy Storage System
SOC	State of Charge
DOD	Depth of Discharge
ECM	Equivalent Circuit Model
LFP	Lithium iron Phosphate
CC	Constant Current
RMSE	Root–Mean–Square Error
OCV	Open-Circuit Voltage
EECM	Equivalent Element Capacitor Model

References

1. Singha, S.; Singha, R. Advancements in Battery and Energy Storage Materials: Paving the Way for Sustainable Energy Solutions. In *Innovations in Next-Generation Energy Storage Solutions*; Mhadhbi, M., Ed.; IGI Global Scientific Publishing: Hershey, PA, USA, 2025; pp. 451–488.
2. Figgener, J.; Stenzel, P. The development of stationary battery storage systems in Germany—A market review. *J. Energy Storage* **2020**, *29*, 101153. [CrossRef]
3. Malhotra, A.; Battke, B.; Beuse, M.; Stephan, A.; Schmidt, T.S. Use cases for stationary battery technologies: A review of the literature and existing projects. *Renew. Sustain. Energy Rev.* **2016**, *56*, 705–721. [CrossRef]
4. Renewable Energy Institute, Battery Storage to Efficiently Achieve Renewable Energy Integration. 2023. Available online: https://www.renewable-ei.org/pdfdownload/activities/REI_BatteryStorage_EN.pdf (accessed on 10 February 2025).
5. Tawfik, M.I.; Ali, A.; Asfoor, M. A combined trade-off strategy of battery degradation, charge retention, and driveability for electric vehicles. *Sci. Rep.* **2024**, *14*, 21995. [CrossRef] [PubMed]
6. Yarimca, G.; Cetkin, E. Review of Cell Level Battery (Calendar and Cycling) Aging Models: Electric Vehicles. *Batteries* **2024**, *10*, 374. [CrossRef]
7. Leng, F.; Tan, C.; Pecht, M. Effect of Temperature on the Aging Rate of Li Ion Battery Operating above Room Temperature. *Sci. Rep.* **2015**, *5*, 12967. [CrossRef] [PubMed]
8. Stroebl, F.; Petersohn, R.; Schricker, B.; Schaeufl, F.; Bohlen, O.; Palm, H. A multi-stage lithium-ion battery aging dataset using various experimental design methodologies. *Sci. Data* **2024**, *11*, 1020. [CrossRef] [PubMed]
9. Roy, A.; Meshram, S.; Patil, R.B.; Arun, S.; Kore, A. Life cycle testing and reliability analysis of prismatic lithium-iron-phosphate cells. *Int. J. Sustain. Energy* **2024**, *43*, 2337439. [CrossRef]
10. Madani, S.S.; Shabeer, Y.; Allard, F.; Fowler, M.; Ziebert, C.; Wang, Z.; Panchal, S.; Chaoui, H.; Mekhilef, S.; Dou, S.X.; et al. A Comprehensive Review on Lithium-Ion Battery Lifetime Prediction and Aging Mechanism Analysis. *Batteries* **2025**, *11*, 127. [CrossRef]
11. Möller, M.; Kucevic, D. SimSES: A holistic simulation framework for modeling and analyzing stationary energy storage systems. *J. Energy Storage* **2022**, *49*, 103743. [CrossRef]
12. Battery Design from Chemistry to Pack—Thermal. Available online: https://www.batterydesign.net/thermal/ (accessed on 15 February 2025).
13. Wang, J.; Liu, P. Cycle-life model for graphite-$LiFePO_4$ cells. *J. Power Sources* **2011**, *196*, 3942–3948. [CrossRef]

14. Xiong, R.; Wang, P.; Jia, Y.; Shen, W.; Sun, F. Multi-factor aging in Lithium Iron phosphate batteries: Mechanisms and insights. *Appl. Energy* **2025**, *382*, 125250. [CrossRef]
15. Luo, G.; Zhang, Y.; Tang, A. Capacity Degradation and Aging Mechanisms Evolution of Lithium-Ion Batteries under Different Operation Conditions. *Energies* **2023**, *16*, 4232. [CrossRef]
16. Wang, T.; Wang, H.; Shen, X.; Lu, C.; Pei, L.; Xu, Y.; Wang, W.; Li, H. Review of Aging Mechanism and Diagnostic Methods for Lithium-Ion Batteries. *Energies* **2025**, *18*, 3884. [CrossRef]